MHD VISCOELASTIC NANOFLUID FLOW UPON AN INCLINED STRETCHING SHEET WITH RADIATION, CHEMICAL REACTION AND MULTIPLE SLIP EFFECTS-HOMOTOPY ANALYSIS METHOD

Saila Kumari PENNELLI [1], Mohammed Ibrahim SHAIK [2*], Vijaya Kumar PRATHI [3]

[1]Research Scholar, Department of Mathematics, Koneru Lakshmaiah Education Foundation, Green Fields, Vaddeswaram 522302, India

[2]Department of Mathematics, Koneru Lakshmaiah Education Foundation, Green Fields, Vaddeswaram 522302, India
[3]Department of Mathematics, GITAM (Deemed to be University), Visakhapatnam, Andhra Pradesh 530045, India
[*]Corresponding author: Shaik Mohammed Ibrahim, ibrahimsvu@gmail.com

An investigation into the computational analysis of magnetohydrodynamic (MHD) flow of a viscoelastic nanofluid (Walters' B' model) over an inclined stretching surface is being carried out in this study. The investigation takes into account numerous slip effects, thermal radiation, and chemical processes. In order to generate the governing partial differential equations (PDEs), similarity transformations are utilized. These equations are then translated into nonlinear ordinary differential equations (ODEs). Utilising the homotopy analysis method (HAM) is the means by which the numerical solution is produced. For the purpose of illustrating the influence of various flow parameters on the effects of magnetic field, thermal radiation, viscoelasticity, chemical reaction rate, and slip effects on momentum, thermal, and solutal curves, a graphical display of the numerical examination is performed at the end of the process. Significant affects of these parameters on the properties of fluid flow, heat and mass transfer are demonstrated by the findings, which have significance for applications in both the industrial and biological fields.

Keywords :Viscoelastic Nanofluid, MHD, Inclined Stretching Sheet, Chemical Reaction, Multiple Slip Effects, Numerical Simulation, Thermal Radiation.

1. Introduction

Viscoelastic fluids are a distinctive type of non-Newtonian fluid that display both elasticity and viscosity, when exposed to stress or deformation. They combine the resistance to shear stress seen in fluids with the ability of solids to recover their original shape. Common examples include blood, honey, ketchup, polymer melts, bitumen, drilling fluids, and personal care products such as cosmetic creams and lotions, chemical processing and manufacturing, oil and gas exploration and production, Polymer manufacturing and processing, Aerospace engineering and manufacturing. Certain elastico-viscous fluids cannot be accurately represented by Maxwell's or Oldroyd's constitutive relations. This is the case for many of these fluids. A category that falls into this category is the Walters B′ fluid Walters [1]. The features of a Walters B′ viscoelastic fluid Walters are believed to be accurately exhibited by a mixture of poly methyl methacrylate and pyridine at a temperature of 25 degrees Celsius, with a polymer content of 30.5 grams per liter and a density of 0.98 grams per liter [2]. In addition to the production of contact lenses, spacecraft, airplanes, tires, belt conveyors, ropes, cushions, seats, foams, and plastic engineering equipment, polymers are also used in the production of

a wide variety of other products. A significant number of these crucial and frequently utilized items are manufactured using the Walters B′ viscoelastic fluid serving as the base. In a diverging channel for physiological fluid flow, Kumar et al. [3] investigated the impact of viscoelastic fluid and surface roughness on the flow of fluid. An investigation into the influence of viscoelastic fluid in a porous media under an electric field within an asymmetric microchannel was carried out by Pandey et al. [4] not too long ago. The significance of visco-elastic electrically conductive motion and materials that vary over time was investigated by Shao et al. [5], who found that these factors outweigh the gravitational impact on the surface of a capsule.

Nanofluids are formed by suspending nanoparticles with typical diameters ranging from 1 to 100 nm. [6] found that even a small concentration of nanoparticles (typically less than 5%), when uniformly dispersed and stably suspended in base fluids, can significantly improve the fluid's thermal conductivity and heat transfer coefficient. Nanotechnology has made enormous advances in applications over the last two decades, solidifying its position as a cornerstone of 21st-century science, technology, and biomechanics. It has numerous uses in a variety of industries, including solar energy collection, sophisticated nuclear systems, electronics, medical technology, biological materials, engine cooling, and heat exchangers. Initially, research on thin liquid film flow focused on fluids with some viscosity, which resulted in viscosity-based classifications that finally saturated the field. Non-Newtonian fluids are studied under varying internal and external influences. Non-Newtonian fluid flow plays a crucial role not only in geophysical phenomena such as mud floods, and lava flows, but also in numerous industrial applications, including biomedical engineering, material processing, and the food and chemical industries. Fluids are classed as Newtonian or non-Newtonian based on their viscosity behaviour, according to Nabwey et al. [7] While Newtonian fluids have a constant viscosity proportional to shear rate, non-Newtonian fluids, the focus of this review, have variable viscosity that changes dynamically in response to shear rate changes.

Magnetohydrodynamics (MHD) studies the behavior of electrically conductive fluids in the presence of a magnetic field, either externally applied or caused by the fluid's motion. Application areas for these flows are extremely diverse and include the casting of steel in industry, heat exchangers which is often called a steam generator in nuclear fusion reactors, bio plasma, medicine, and nanotechnology, to name a few. In a wide variety of industrial processes, electrically conductive fluids play a significant role. Notable examples of such fluids include liquid metals such as aluminum, mercury, and crucible steel. Diverse MHD events are produced because of the interaction of a flowing fluid with a magnetic field. These events can be utilized in a variety of different ways. Electromagnetic flow control is utilized in industrial processes for the purpose of stabilizing molten metals, managing free surfaces, and producing fine powders, semiconductors, aluminum, and high-performance super alloys. The development of fusion reactors, which use high-intensity magnetic fields to control plasma, is driving much of the current interest in MHD research. Electromagnetohydrodynamic (EMHD) flows are effective for transporting low-conductivity fluids in microsystems. Viscoelastic nanofluid flows have numerous applications in the fields of biomedical engineering, energy systems, and materials science. These microfluidic devices provide precise fluid movement for a variety of applications, including enhancing the velocity of one fluid through interaction with another fluid, promoting efficient heat transfer, and allowing for regulated fluid mixing that can be controlled. Understanding these fluids' complex dynamics is critical for developing new medication delivery systems, electronic cooling devices, and heat exchangers. The roots of MHD are sometimes traced to the pioneering work of Hartmann [8] conducted the first liquid metal experiments in 1937. Julius Hartmann made additional contributions to the advancement of technology by attempting to design an electromagnetic conduction pump for the purpose of moving fluids that are electrically conductive. Following their findings, a few researchers looked into cases like the Couette flow of a conductive viscous fluid between two parallel plates under perpendicular magnetic field Agarwal et al. [9] & Lehnert [10] Hartmann’s research found that magnetic fields and induced currents greatly affect swiftness contours, resulting in boundary layers with high velocity gradients near the plates. The diverse range of electrically conductive fluids provides numerous options for the development of MHD applications. Nanofluids are one type of fluid that received a lot of interest in the second part of the twentieth century. Nayak et al.[11] studied MHD viscoelastic fluid flow in a porous material using Walters' B' fluid model, adding to the growing body of research in this

area. Thermal radiation, commonly known as heat radiation, is the electromagnetic radiation released by an object or material as a function of its temperature. It is a type of energy transfer that occurs when a hotter body emits energy into its cooler surroundings. The author Singh et al.[12] examined the effects of heat radiation and other thermophysical parameters on fluid movement. Many research scholars have studied the importance of MHD and thermal radiation effects on nanofluids and non-Newtonian fluids (see [13-16]).

Chemical reactions take place when two components meet and produce a product in the presence of an aiding factor, such as a catalyst. These reactions are divided into two categories: reversible and irreversible. Irreversible reactions cannot be reversed, but reversible reactions can move forward and backward. Swarnalathamma et al.[17] investigated the effects of radiation absorption and chemical reactions on MHD free convective Casson fluid flow via an infinite, vertically inclined porous plate. Krishna et al. [18] studied the unsteady MHD third-grade fluid flow across a high-temperature shrinking sheet embedded with silver nanoparticles and affected by nonlinear radiation. Popoola et al. [19] used numerical analysis to investigate the effect of chemical reactions on MHD viscoelastic fluid flow. Mahapatra et al. [20] investigated the impact of chemical reactions on free convection flow in a porous material near a vertical surface. Furthermore, Mohamed et al.[21] explored Walters'-B nanofluid mixed convection flow and thermal transfer around a circular cylinder in the presence of thermal radiation.

The phenomenon of no-slip boundary conditions in fluid flow phenomena has been investigated by a number of researchers. The macroscopic slip property is shown by certain fluids, including liquid polymers, foams, and emulsions, among others. Both the temperature and the velocity of these fluids diverge from the surface when they are in close proximity to solid particles. There are a wide variety of applications for fluid flows that demonstrate high slip effects. These applications include fluid movement in inner body cavities as well as several industrial and engineering processes. According to Seid et al. [22], the optimal homotopy technique was utilized in order to study the influence that various slip circumstances have on MHD unsteady viscoelastic nanofluid flow across a sheet that is expanding vertically while radiation was present. Several slip effects were shown to be responsible for the expansion of boundary layers, according to their findings. Multiple slip effects are the subject of more research, which may be found in [23-26]. In the manufacturing business as well as in other technological applications, increasing the efficiency of heat transfer is a major goal. An increase in heat transmission not only makes it possible to produce industrial goods of a higher quality at a lower cost, but it also helps to reduce the amount of damage that can be caused by devices overheating.

The employment of the homotopy analysis method (HAM), which was presented by Zhu and Granick [27], leads to the achievement of the objective of acquiring the required analytical response. With the assistance of this method, which has seen broad use, a number of distinct issues involving heat transfer and fluid dynamics have been resolved. Both HAM and an exponentially stretched surface were applied by researchers [28-30] in order to accomplish the goals of evaluating nanofluid flow and proposing analytical solutions. Furthermore, additional study [31-34] was conducted to investigate the nonlinear thermal radiation properties of polymeric materials. The HAM technique was utilized to analyze the results of this investigation. Ishak et al. [35] did research in the past to investigate the impact of heat and mass transfer in the flow of a viscoelastic nanofluid across a stretching sheet while the sheet was subjected to velocity slip conditions. The research was carried out in order to investigate the significance of these two factors.

The studies that are now being conducted investigate the ways in which viscoelastic nanofluid flow is affected by magnetohydrodynamics, heat radiation, chemical reactions, and slip conditions. The homotopy analysis approach, also known as HAM, was utilized in order to derive numerical solutions for the nonlinear ODEs and boundary conditions that were produced as a result. Comparisons of fundamental physical characteristics are depicted through the use of graphical representations. This method is also utilized for the purpose of determining significant technical metrics, such as the Sherwood number, the Nusselt amount, and the skin friction coefficient. Magnetic fields, non-Newtonian fluid dynamics, and heat transfer are all components that interact with one another, and the

findings shed significant light on this relationship. The optimization of industrial processes and the improvement of engineering systems are both significantly impacted by these discoveries, which have significant ramifications.

Research question

i. How do thermal radiation and heat source influence the boundary layer flow and features of thermal transmission of visco-elastic nanofluids?

ii. What is the impact of Brownian motions and thermophoresis's on the flow, thermal, and concentration profiles of visco-elastic nanofluids in the presence of multiple slip effects?

iv. In what ways can magnetohydrodynamics (MHD) enhance or reduce the efficiency of heat transfer in visco-elastic nanofluids?

v. How can the HAM technique solver be utilized effectively to predict the implication of visco-elastic fluid factors on thermal and flow distributions?

vi. What is the role of Schmidt number and Prandtl number in optimizing heat transfer and flow dynamics in a visco-elastic nanofluid system?

2. Formulation of the problem

The fluid transport properties of an incompressible MHD viscoelastic nanofluid will be explored over a porous extended sheet that is inclined perpendicular to its vertical axis. These properties will be modified by chemical processes. By using boundary conditions that are convective, additionally assessed are heat generation and absorption. As shown in Fig. 1, the X- and Y-axes are parallel to the surface and aligned along the inclined surface. Stretching has been achieved by moving the wall with a velocity $U_w = ax$, ,along the x-axis. The MHD, thermal, as well as the concentration boundary layers are supposed to develop along the y-axis, and grow along the x-axis. We have T_w for temperature close to the surface and T_∞ for temperature far from the surface, and C_w and C_∞ for concentration, respectively. For the purpose of the flow analysis, the fluid is subjected to a normal-to-flow magnetic field with an intensity of B_0. Brownian motion characteristics are taken into account. Thermal radiation, chemical reactions, heat sources, and multi-slip effects are all discussed.

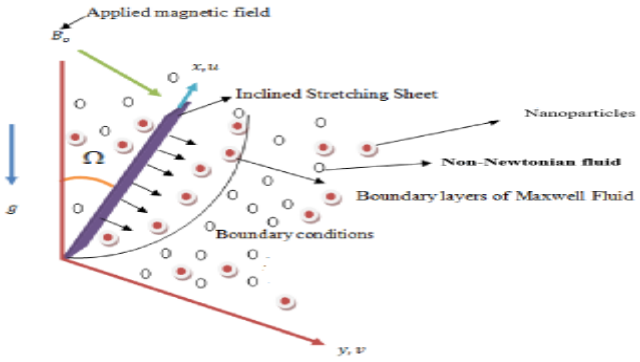

Fig.1 Modelling of the flow geometry

Within the bounds of the boundary layer approximations, the following equations regulate the conservation of mass, momentum, thermal energy, and nanoparticle concentration (see [35]):

$$u_x + v_y = 0 \tag{1}$$

$$uu_x + vu_y = vu_{yy} - \frac{k_0}{\rho}\left(uu_{xyy} + uu_x u_{yy} + u_y v_{yy} + vu_{yyy}\right) - \frac{\sigma B_0(x)^2}{\rho}u$$
$$-g\left[-\beta_T\left(T - T_\infty\right) - \beta_C\left(C - C_\infty\right)\right]\cos\Omega \tag{2}$$

$$uT_x + vT_Y = \frac{k}{(\rho c)_f} T_{yy} + \tau\left[D_B C_y T_y + \frac{D_T}{T_\infty}\left(T_y\right)^2 \right] + \frac{Q_0}{(\rho c)_f}\left(T - T_\infty\right) - \frac{1}{(\rho c)_f}\, q_{ry}, \tag{3}$$

$$uC_x + vC_y = D_B\left(C_{yy}\right) + \frac{D_T}{T_\infty}\left(T_{yy}\right) - Kr\left(C - C_\infty\right). \tag{4}$$

$$\begin{aligned} &u = U_w(x) + \delta_1^*\left(u_y\right),\ v = 0,\ T = T_w(x) + \delta_2^*\left(T_y\right),\ C = C_w(x) + \delta_3^*\left(C_y\right) \text{ at } y = 0 \\ &u \to U_\infty, \qquad T \to T_\infty,\ C \to C_\infty, \qquad \text{as} \qquad y \to \infty, \end{aligned} \tag{5}$$

where $\upsilon = \frac{\mu}{\rho_f}$, $\tau = \frac{(\rho c)_p}{(\rho c)_f}$.

Following Roseland approximation, the radiative heat flux is

$$q_r = -\frac{4\sigma^*}{3\kappa^*}\frac{\partial T^4}{\partial y}, \tag{6}$$

where Stefan Boltzmann constant is σ^* and κ^* is the mean absorption coefficient. Moreover, we assume that the flow's internal temperature differential is adequately large so that T^4 is represented as a linear function of thermal As a result, by expanding T^4 in Taylor series about T_∞ and if we ignore terms of higher order, we get

$$T^4 \cong 4T_\infty^3 T - 3T_\infty^4, \tag{7}$$

Using Equations (6) and (7) the Equation (3) converts into:

$$u\frac{\partial T}{\partial x} + v\frac{\partial T}{\partial y} = \left(\frac{\kappa}{(\rho c)_f} + \frac{16\sigma^* T_\infty^3}{3\kappa^*(\rho c)_f}\right)\frac{\partial^2 T}{\partial y^2} + \tau\left[D_B\frac{\partial C}{\partial y}\frac{\partial T}{\partial y} + \frac{D_T}{T_\infty}\left(\frac{\partial T}{\partial y}\right)^2 \right] + \frac{Q_0}{(\rho c)_f}\left(T - T_\infty\right), \tag{8}$$

using the following similarity transformations to reduce the PDE's into ODE's:

$$u = axf'(\zeta), v = -\sqrt{av}\, f(\zeta), \theta(\zeta) = \frac{T - T_\infty}{T_W - T_\infty}, \phi(\zeta) = \frac{C - C_\infty}{C_W - C_\infty}, \zeta = \sqrt{\frac{a}{v}}y, \tag{9}$$

where ζ is the similarity variable.

Substitute the equation (9) in the equations (2), (4) and (8), we get

$$f''' + ff'' - f'^2 + k_1\left(ff^{iv} - 2ff''' + f''^2\right) - Mf' + \left(Gr\theta + Gc\phi\right)\cos\Omega = 0,$$

$$(10)\left(1 + \frac{4}{3}R\right)\theta'' + \Pr f\theta' + \Pr Nb\,\phi'\theta' + \Pr Nt\,\theta'^2 + \Pr Q\theta = 0,$$

$$(11)\ \phi'' + Sc\left(f\phi' - \gamma\phi\right) + \frac{Nt}{Nb}\theta'' = 0.$$

(12)

The boundary conditions are

$$\begin{aligned} &f(0) = 0,\ f'(0) = 1 + \delta_1 f''(0), \theta(0) = \left(1 + \delta_2\theta'(0)\right),\ \phi(0) = \left(1 + \delta_3\phi'(0)\right), \\ &f'(\infty) \to 0, \theta(\infty) \to 0, \phi(\infty) \to 0, \end{aligned} \tag{13}$$

where

$$k_1 = \frac{k_0 a}{\nu}, \qquad M = \frac{\sigma_f B_0^2}{\rho_f a}, \qquad Gr_x = \frac{g\beta_T\left(T_w - T_\infty\right)x^3}{\upsilon^2}, \qquad Gr = \frac{Gr_x}{\mathrm{Re}_x^2}, \qquad Gc_x = \frac{g\beta_C\left(C_w - C_\infty\right)x^3}{\upsilon^2},$$

$$Gc = \frac{Gc_x}{\mathrm{Re}_x^2}\,\mathrm{Re}_x = \frac{U_w x}{\upsilon} = \frac{ax^2}{\upsilon}, \quad \Pr = \frac{\upsilon}{\alpha}, \quad Nb = \frac{\tau D_B\left(C_w - C_\infty\right)}{\nu}, \quad Nt = \frac{\tau D_T\left(T_w - T_\infty\right)}{\upsilon T_\infty}, \quad R = \frac{4\sigma^* T_\infty^3}{k^* k},$$

$$Q = \frac{Q_0}{a(\rho c)_f}, \quad Sc = \frac{\upsilon}{D_B}, \quad \gamma = \frac{Kr}{a}, \quad \delta_1 = \delta_1^*\sqrt{\frac{a}{\upsilon}}, \quad \delta_2 = \delta_2^*\sqrt{\frac{a}{\upsilon}}, \quad \delta_3 = \delta_3^*\sqrt{\frac{a}{\upsilon}}$$

The essential quantities of interest are the skin-friction factor, local Nusselt number, and the local Sherwood number, that are represented as

$$C_f = \frac{\tau_w}{\rho u_w^2}, Nu_x = \frac{xq_w}{k\left(T_w - T_\infty\right)}, Sh_x = \frac{xj_w}{D_B\left(C_w - C_\infty\right)}$$

The surface shear stress τ_W , surface heat flux q_w and surface mass flux j_w are represented

$$\tau_w = \mu\left(\frac{\partial u}{\partial y}\right)_{y=0} - k_0\left(u\frac{\partial^2 u}{\partial x\partial y} + v\frac{\partial^2 u}{\partial y^2} - 2\frac{\partial u}{\partial y}\frac{\partial v}{\partial y}\right)_{y=0}, q_w = \left(-\left(k_\infty + \frac{16\sigma^* T_\infty^3}{3k^*}\right)\left(\frac{\partial T}{\partial y}\right)\right)_{y=0},$$

by

$$j_m = -D_B\left(\frac{\partial C}{\partial y}\right)_{y=0}.$$

Using Eq. (9), we get

$$C_f\,\mathrm{Re}_x^{1/2} = \left[1 - 3k_1 f'(0)\right] f''(0), Nu_x\,\mathrm{Re}_x^{-1/2} = -\left(1 + \frac{4R}{3}\right)\theta'(0), Sh_x\,\mathrm{Re}_x^{-1/2} = -\phi'(0). \quad (14)$$

3.Solution methodology and Convergence of HAM

HAM

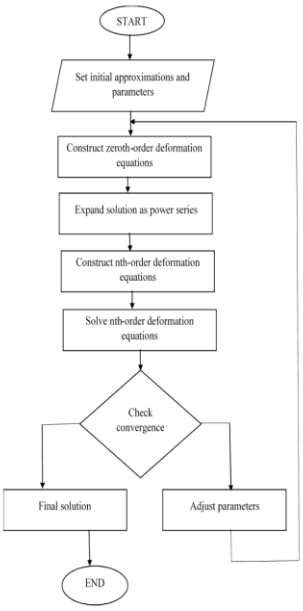

Figure 2. Diagrammatic representation of HAM process.

It is demonstrated that the Homotopy Analysis Method (HAM), also known as the Homotopy Analysis Method, is an effective semi-analytical method by the fact that it is utilized in a variety of research projects to handle boundary layer flow issues. As an illustration, it has been successfully utilized to acquire semi-analytical solutions for the thermal convection boundary layer flow of incompressible Casson fluids. These solutions incorporate features such as suction/injection and heat sink effects, both of which are essential in polymer coating applications. In addition, the ability of HAM to handle non-linear boundary value problems has been demonstrated by the fact that it has been utilized to produce mathematical expressions for velocity, heat and mass transfer in boundary layer flows that involve thermal radiation in presence of multiple slip effects. The approach has also been utilized in the field of magnetohydrodynamics, which has shed light on the impact that parameters like magnetic and Prandtl numbers have on flow characteristics. Additionally, the BVPh2.0 program has the capability to ease the implementation of HAM, which enables the efficient computing of solutions in complicated boundary layer situations that involve nanofluids and Casson fluids.

Employing the HAM allowed us to derive the analytic solutions for Eqs. (10)–(12) with the prescribed boundary conditions (13), using selected initial guesses and linear operators for the functions f, θ, and ϕ.

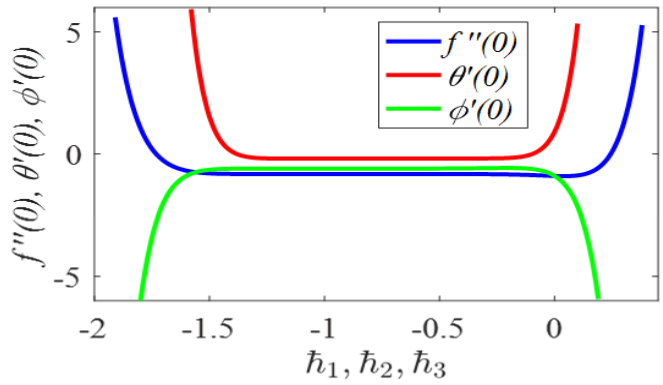

Fig. 2. $\hbar$-curves for $f''(0), \theta'(0)$ and $\phi'(0)$ at 15th order approximations.

Table 1. Convergence of HAM solution with various orders of approximations at $k_1 = 0.1, M = 0.5, \Omega = 60^o, R = \delta_1 = \delta_2 = \delta_3 = Q = Gr = Gc = 0.1, \Pr = 1.4, Sc = 1.0, Nb = 0.3, Nt = 0.2, \gamma = 0.2.$

Order	$-f''(0)$	$-\theta'(0)$	$-\phi''(0)$
5	-1.020448	0.333042	0.578612
10	-1.019805	0.317650	0.587336
15	-1.019759	0.315833	0.588758
20	-1.019757	0.315697	0.588903
25	-1.019757	0.315721	0.588896
30	-1.019757	0.315735	0.588888
35	-1.019757	0.315738	0.588885
40	-1.019757	0.315738	0.588885
45	-1.019757	0.315738	0.588885

4. Results and Discussion

The graphs are intended to examine the impact of physical features on momentum, thermal, and solutal. This section emphasizes the graphical representation of the physical characteristics combined with flow processes. A comparison with historical patterns was conducted to verify the accuracy of our endeavor, resulting in significant concordance, as illustrated in Table 2. Unless otherwise mentioned in the related figures, we strictly stick to the values given in Table 1 so that the numerical results of this study are consistent.

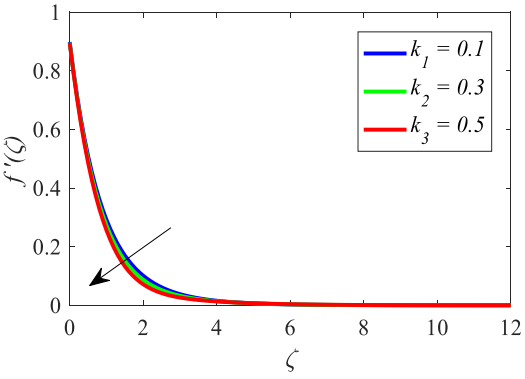

Fig. 4. Outlines of $f'(\zeta)$ for k_1.

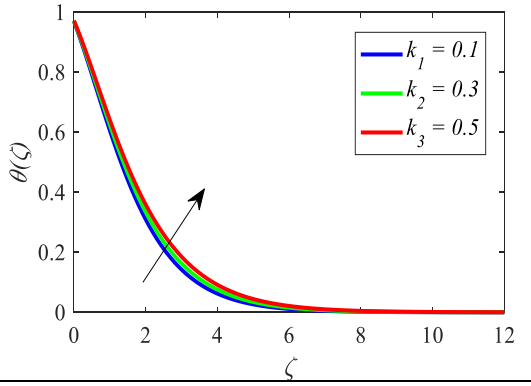

Fig. 5 Outlines of $\theta(\zeta)$ for k_1.

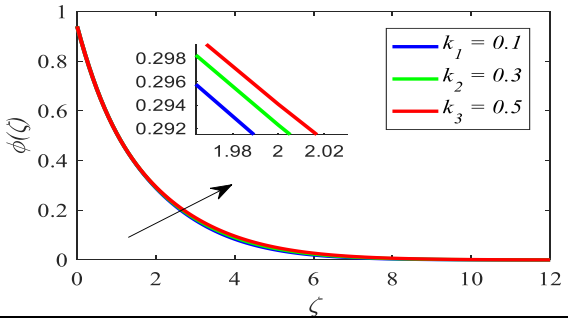

Fig. 6. Outlines of $\phi(\zeta)$ for k_1.

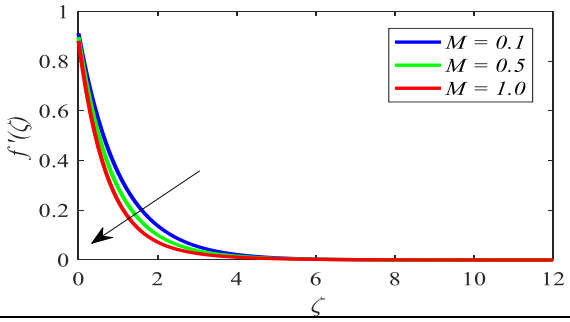

Fig. 7. Outlines of $f'(\zeta)$ for M.

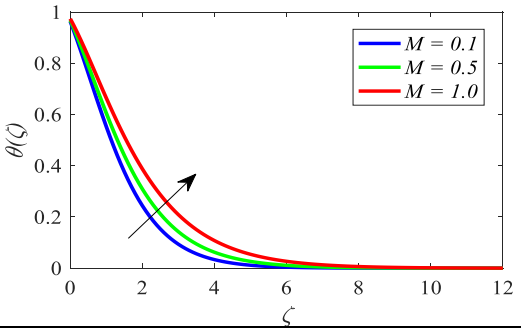

Fig. 8. Outlines of $\theta(\zeta)$ for M

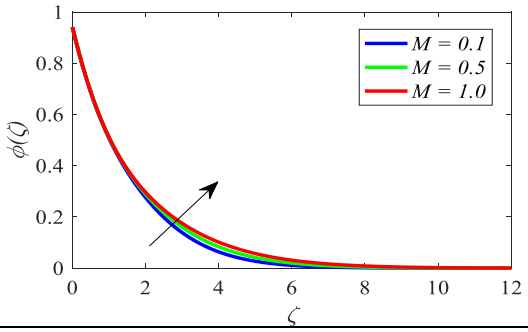

Fig. 9. Outlines of $\phi(\zeta)$ for M.

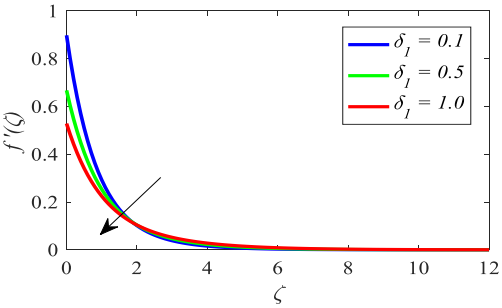

Fig. 10 Outlines of $f'(\zeta)$ for δ_1

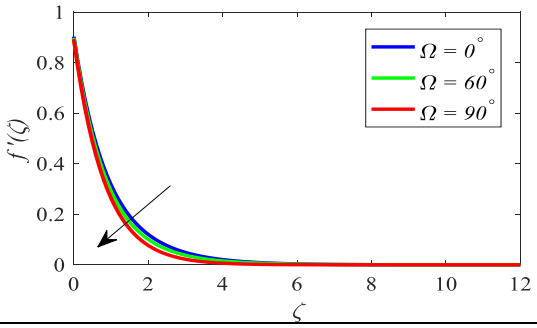

Fig. 11. Outlines of $f'(\zeta)$ for Ω.

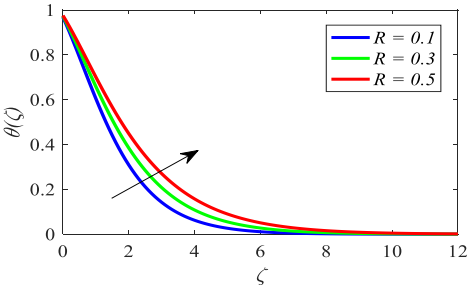

Fig. 12. Outlines of $\theta(\zeta)$ for R.

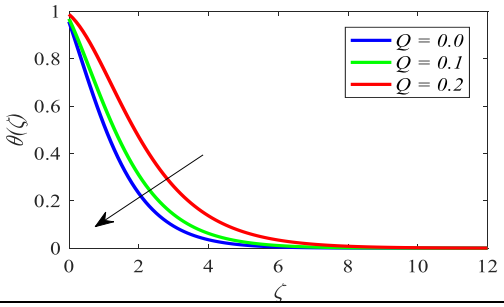

Fig. 13. Outlines of $\theta(\zeta)$ for Q.

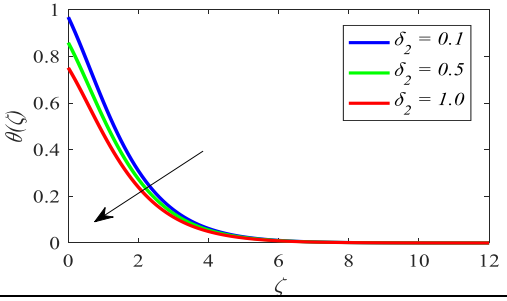

Fig. 14. Outlines of $\theta(\zeta)$ for δ_2.

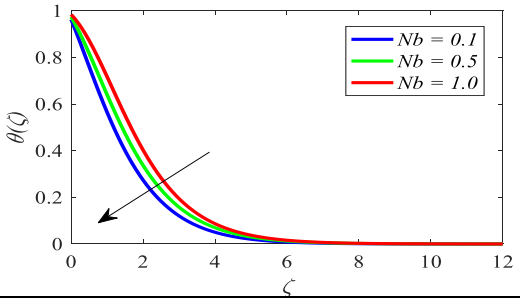

Fig. 15 Outlines of $\theta(\zeta)$ for Nb.

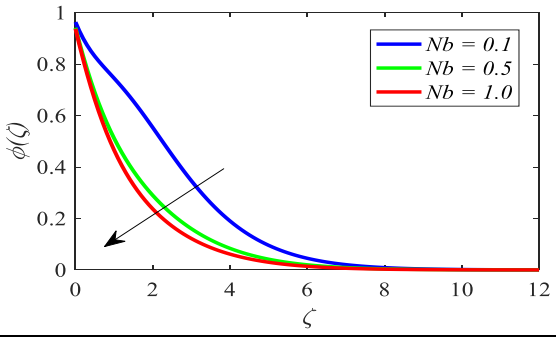

Fig. 16 Outlines of $\phi(\zeta)$ for Nb.

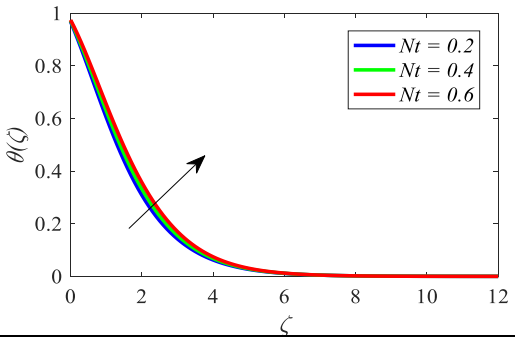

Fig. 17 Outlines of $\theta(\zeta)$ for Nt.

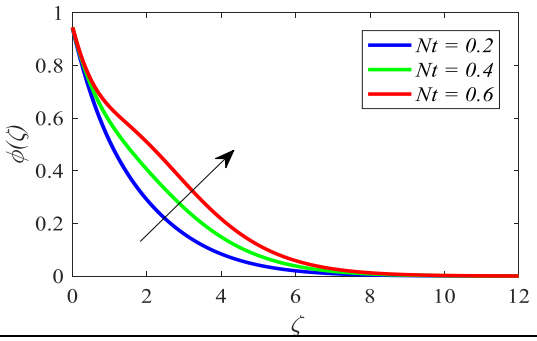

Fig. 18. Outlines of $\phi(\zeta)$ for *Nt*.

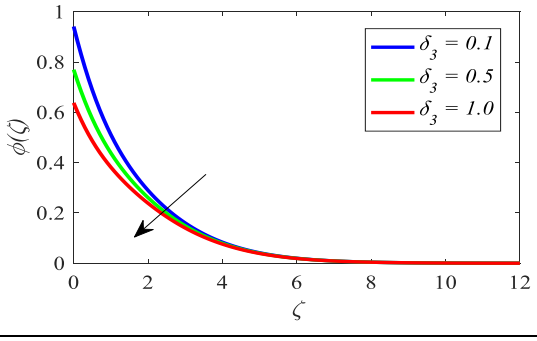

Fig. 19. Outlines of $\phi(\zeta)$ for δ_3.

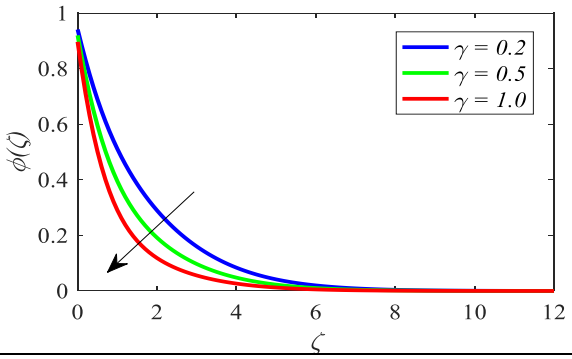

Fig. 20. Outlines of $\phi(\zeta)$ for γ.

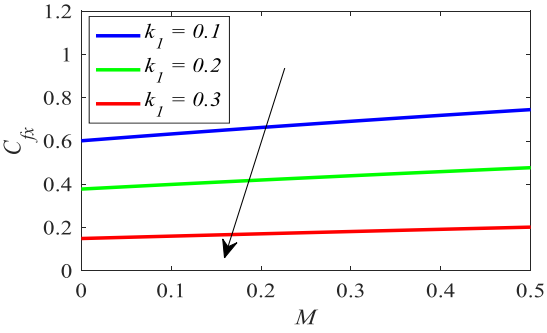

Fig. 21. Outlines of C_{fx} for k_1 and M.

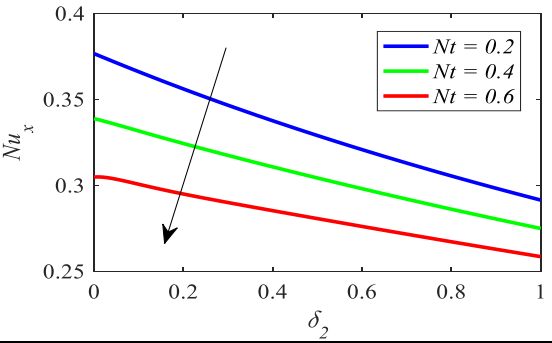

Fig. 22 Outlines of Nu_x for *Nt* and δ_2.

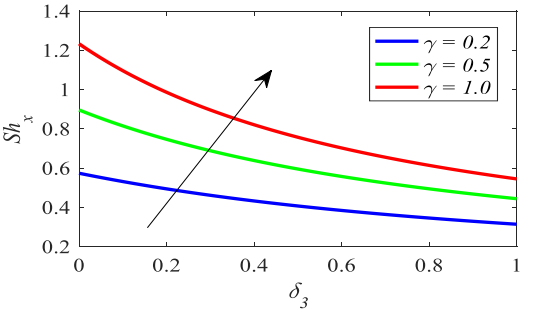

Fig. 23 Outlines of Sh_x for δ_3 and γ.

The effects of the viscoelastic parameter k_1 on the flow of the fluid and the temporal distribution of heat and mass are shown in Figures 4-6. The graph shows that as k_1 gets greater, fluid motion gets worse close to the stretched sheet and better further away. Furthermore, heat transfer is reduced as the second-grade parameter is increased, since fluid movement is accelerated. Consequently, when viscoelastic effects intensify, the momentum boundary layer enlarges while the thermal and concentration boundary layers contract. Figures 7-9 demonstrate the influence of

magnetic constraint *M* on the contours. Notably, f'(ζ) decreases as *M* upsurges, whereas the opposite trend is observed for thermal and solutal contours. This phenomenon occurs because the Lorentz force, which hinders fluid motion, intensifies with increasing , resulting in a decline in transport rate. Upon applying the magnetic field to the flow field, the Lorentz force becomes significant, slowing down the fluid flow and increasing drag. Consequently, the fluid flow momentum declines as the momentum layer thickness upsurges. Figure 10 shows how the flow distribution is affected by the flow slip limitation δ_1. It is evident from the analysis that the increase in the flow slip constraint δ_1, representing the speed contour, decreases. Snowballing the slip parameter clearly results in a diminishing swiftness. Figure 11 reveals that the momentum of the fluid declines as the inclination angle Ω upsurges. This reduction in velocity is attributed to the presence of Lorentz forces near the solid surface, which alter the flow pattern and consequently lead to a decline in fluid velocity.

Figure 12 demonstrates that an increase in the radiation constraint *R* leads to a corresponding upsurge in the dimensionless temperature. This phenomenon occurs because enhanced thermal radiation results in a higher rate of heat absorption by the fluid particles, leading to increased thermal energy retention. Consequently, the local temperature distribution, or thermal contour, across the fluid exhibits a significant rise. Notably, this effect is particularly pronounced in high-temperature systems, where radiative heat transfer becomes the dominant mode of energy transmission.

Figure 13exemplifies the remarkable impact of Q on θ(ζ). In the instance of air, an upsurge in the values improves θ. After declining at first, the thermal contour rises away from the wall.Figure 14 demonstrates that the temperature declines as the thermal slip constraint δ_2 rises, resulting in a reduced physical width of the thermal boundary layer despite minimal heat transfer from the sheet to the fluid.The effect of the Brownian motion constraint *Nb* on the thermal contour is depicted in Fig. 15 The results indicate that as *Nb* increases, the distance between the thermal boundary layers declines. Furthermore, Fig. 16 illustrates the relationship between the concentration distribution and *Nb*, revealing that the concentration boundary layer thickness decreases with increasing *Nb* values. Notably, the graphical representation also shows that the thermal boundary layer thickness declines despite increasing *Nb* values, providing valuable insights into the system's behaviour. Figs. 17 and 18 are dedicated to investigating the impact of thermophoresis *Nt* on thermal and solutal contours. Based on the available data, it can be inferred that increasing thermophoresis *Nt* values lead to a widening gap between the thermal and concentration boundary layers, indicating a growing distance between these boundaries. Figure 19 shows that the nanoparticle fraction slip constraint δ_3 has a comparable effect on the mass fraction field, mirroring its impact on the thermal field. This similarity arises from the fundamental hindrance to fluid motion caused by slip, leading to diminished molecular progress and, consequently, a decrease in the mass fraction field.

Figure 20 demonstrates the effect of the chemical reaction constraint γ on the solutal contour $\phi(\zeta)$ revealing that an upsurge in γ leads to a declination in the solutal contour.Figure 21 illustrates the variation of the local skin friction coefficient with respect to the visco elastic constraint k_1 and the magnetic constraint *M*. Notably, it is observed that increasing values of k_1 and *M* lead to a decrease in the local skin friction coefficient. Figure 22 displays that the Nusselt number decreases with increasing values of both the thermophoresis constraint *Nt* and the thermal slip constraint δ_2. Fig. 23 displays that local Sherwood number varies with γ and δ_3, it is observed that local Sherwood number is an increasing function of γ and increases with an increases with δ_3.

Table 2 compares the calculated $-\theta'(0)$ values to those from previous studies over various ranges. There is limited consistency between the previous results and the present ones.

Table 2. Comparison of $-\theta'(0)$ for different values of Pr in the absence of remaining parameters

Pr	Ishak *et al.*[31]	HAM
0.72	0.46326	46.3255×10^{-2}
1.0	0.58198	58.1992×10^{-2}
3.0	1.16525	116.5213×10^{-2}

5. Conclusions

We study non-Newtonian nanofluid flow over a elongating sheet with heat source/sink, thermophoresis, and Brownian motion. Using the Homotopy Analysis Method (HAM), we analyze the impact of controlling constraints, including magnetic field effects, on momentum, thermal, and solutal distributions, as well as skin friction, Nusselt number, and Sherwood number. The following conclusions can be drawn from this study are

(i)When the viscoelastic constraint is improved, the thickness of the velocity boundary layer as well as the momentumn decreases, where as, the solutal and thermal upsurges.

(ii)The distribution of flow momentum decreases as the slip of fluid on the stretched surface increases.

(iii)A thinner thermal boundary layer is the outcome of an increase in the heat source constraint, which causes a drop in thermal. A fall in fluid thermal causes an increase in viscosity.

(iv)The nanofluid's viscoelasticity reduces the local skin friction and Nusselt number while increasing the local Sherwood number. (v)The Brownian motion constraint declines on the thermal and nano particle concentration contours, whereas the thermophoresis constraint upsurges on thermal and nano particle concentration.

(vi)The chemical reaction constraint declines on the nano particle concentration.

Terminology: -

Abbreviations	SI units	Abbreviations	SI units
∞ (Free stream)	ms^{-1}	Ω (Inclination angle)	radian (rad)
T_w (convective fluid temperature)	k (kelvin)	(τ_W)surface shear stress	Pascal (Pa).
T_∞ (ambient fluid thermal)	k (kelvin)	κ (Thermal conductivity of fluid)	$wm^{-1}k^{-1}$
μ (Dynamic viscosity)	$kgm^{-1}s^{-1}$	q_r (radiative heat flux)	wm^{-2}
g (Acceleration due to gravity)	ms^{-2}	D_T (Thermophoresis diffusion factor)	m^2s^{-1}
μ_∞ (Infinity viscosity)	nsm^{-2}	γ (Chemical reaction constraint)	ms^{-1}
u,v (Momentum components in x, y directions)	ms^{-1}	j_w (surface mass flux)	$kgm^{-2}s^{-1}$
C ((fluid concentration)	$molm^{-3}$	ρ_f (fluid density)	kgm^{-3}
C_w (solutal level of fluid at surface)	$molm^{-3}$	C_∞ (ambient solutal)	$molm^{-3}$
T (fluid temperature)	k (kelvin)	k_1 (Viscoelastic constraint)	nm^{-2}
$\delta_1, \delta_2, \delta_3$ (Slip factors)	m	D_B (Brownian diffusion factor)	m^2s^{-1}
MHD (Magneto hydro		U_w (Stretching velocity)	

dynamics)			
Q (heat generation factor)		Re_x (Local Reynolds number)	
k^* (absorption coefficient)		ϕ (Concentration of a fluid with no dimension)	
θ (Temperature of a fluid with no dimension)		q_w (Surface heat flux)	
χ_n (Characteristic function)			
α (Thermal diffusivity)		R (Thermal radiation constraint)	
M (Magnetic field constraint)		Sh_x (Local Sherwood number)	
Nt (Thermophoresis constraint)		F (stream function with no dimension)	
Nb (Brownian motion constraint)		F' (swiftness with no dimension)	
Pr (Prandtl number)		Sc (Schmidt Number)	
ψ (Stream function)		ϕ (Concentration of a fluid with no dimension)	
HAM (Homotopy analysis technique)		f (dimension less velocity)	
ρ_p (mass density of nanoparticles)		$(\rho c)_p$ (Nanoparticles heat capacity)	
σ^* (Stefan -Boltzmann constant)		Gc (Solutal local Grashof number)	
D_i^* ($i=1$ to 7) (Random coefficients)		ζ (A variable with no dimension)	
$(\rho c)_f$ (Heat capacity of the fluid		$(c)_f$ (Specific heat at constant pressure)	
Gr (Local Grashof number due to thermal)		$\tau = \frac{(\rho c)_p}{(\rho c)_f}$ (Ratio of Nanofluid Heat Capability to the Base Fluid)	
	Subscripts		
f (fluid)		w (wall)	
a (constant stretching rate)			

References

[1] Walters, K.. The motion of an elastico-viscous liquid contained between coaxial cylinders (II). *The Quarterly Journal of Mechanics and Applied Mathematics*, *13*(4), (1960), pp. 444-461, https://doi.org/10.1093/qjmam/13.4.444

[2] Walters, K.. The solution of flow problems in the case of materials with memory. *J. Mecanique*, *1*(4), (1962), pp. 479-486.

[3] Kumar, A., *et al.,*. Peristaltic pumping of viscoelastic fluid in a diverging channel: effects of magnetic field and surface roughness. *International Journal of Numerical Methods for Heat & Fluid Flow, 13(1),* (2024), pp.23-32. https://doi.org/10.1108/HFF-09-2024-0664

[4] Pandey, A., *et al.,*. Transient flow of electrolyte solution in porous media with membranes fitted at the upper wall surface and lower charged surface. *Microfluidics and Nanofluidics*, *28*(10), (2024), pp. 69, https://doi.org/10.1007/s10404-024-02761-9

[5] Shao, Y., *et al.,*. Heat and mass transfer analysis during Homann Visco-elastic slippery motion of nano-materials. *International Communications in Heat and Mass Transfer*, *139*,(2022),pp.106425. https://doi.org/10.1016/j.icheatmasstransfer.2022.106425

[6] Choi, S. U. S., *et al.,*. Anomalous thermal conductivity enhancement in nanotube suspensions. *Applied physics letters*, *79*(14), (2001), pp. 2252-2254. https://doi.org/10.1063/1.1408272

[7] Nabwey, H. A., *et al.,*. A comprehensive review of non-Newtonian nanofluid heat transfer. *Symmetry*, *15*(2), (2023), pp.362-371. https://doi.org/10.3390/sym15020362

[8] Hartmann, J.. Hydrodynamics I theory of the laminar flow of an electrically conducting liquid in a homogeneous magnetic field. *Kgl Danske VidensKabernes Selskab Math. Fys. Med*, *15*(6), (1937), pp. 123-132.

[9] Agarwal, K. M., *et al.,*. Deformation analysis of Al Alloy AA2024 through equal channel angular pressing for aircraft structures. *Advances in Materials and Processing technologies*, *8*(1), (2022), 828-842. https://doi.org/10.1080/2374068X.2020.1834756

[10] Lehnert, B. O.. *On the behaviour of an electrically conductive liquid in a magnetic field*. Almqvist u. Wiksell. (1952)

[11] Nayak, M. K., *et al.,*. Heat and mass transfer effects on MHD viscoelastic fluid over a stretching sheet through porous medium in presence of chemical reaction. *Propulsion and Power Research*, *5*(1), (2016), pp. 70-80. https://doi.org/10.1016/j.jppr.2016.01.006

[12] Singh, B., *et al.,*. Effect of transverse speed on mechanical and microstructural properties of friction stir welded aluminium AA2024-T351. *Advances in Materials and Processing Technologies*, *6*(3), (2020), pp. 519-529. https://doi.org/10.1080/2374068X.2020.1728642.

[13] Meenakumari, R., Lakshminarayana, P., Vajravelu, K., & Sucharitha, G. (2023). Convective heat and mass transfer analysis on Casson nanofluid flow over an inclined permeable expanding surface with modified heat flux and activation energy. Numerical Heat Transfer, Part A: Applications, 86(6), 1515–1534. https://doi.org/10.1080/10407782.2023.2275281

[14] Ilango, M.S., Lakshminarayana, P. Induced magnetic field and Soret–Dufour effects on viscous dissipative Casson fluid flow through porous medium over a stretching sheet. *J Therm Anal Calorim* **149**, 8713–8727 (2024). https://doi.org/10.1007/s10973-024-13352-9

[15] Vajravelu, K., Abraham, J. P., Mukhopadhyay, S., Lakshminarayana, P., & Sundén, B. (2024). Advances in nanofluid flow, heat, and mass transfer at moving/stretching surfaces. *Advances in Heat Transfer*, *58*, 81. https://doi.org/10.1201/9781003571278

[16] Meenakumari, R., Sucharitha, G., Pallavarapu, L., & Vajravelu, K. (2024). Darcy-Forchheimer flow of a conducting micropolar fluid at a stretching sheet with convective boundary conditions. *Journal of Porous Media*, *27*(5). **DOI:** 10.1615/JPorMedia.2023045629.

[17] Swarnalathamma, B. V., *et al.,*. Combined impacts of radiation absorption and chemically reacting on MHD free convective casson fluid flow past an infinite vertical inclined porous plate. *Journal of Computational Mathematics and Data Science*, *5*, (2022), 100069. https://doi.org/10.1016/j.jcmds.2022.100069

[18] Krishna, M. V., *et al.,*. Unsteady MHD third-grade fluid past an absorbent high-temperature shrinking sheet packed with silver nanoparticles and non-linear radiation. *Journal of Taibah University for Science*, *16*(1), (2022), 585-593. https://doi.org/10.1080/16583655.2022.2087396

[19] Popoola, A. O., *et al.,*. Heat and mass transfer on MHD viscoelastic fluid flow in the presence of thermal diffusion and chemical reaction. *International Journal of Heat and Technology*, *34*(1), (2016), pp. 15-26. https://doi.org/10.18280/ijht.340103

[20] Mahapatra, N., *et al.,*. Effects of chemical reaction on free convection flow through a porous medium bounded by a vertical surface. *Journal of Engineering Physics and Thermophysics*, *83*, (2010), pp.

130-140. https://doi.org/10.1007/s10891-010-0327-1
[21] Mohamed, R. A., *et al.*,. MHD Casson nanofluid flow over a stretching surface embedded in a porous medium: effects of thermal radiation and slip conditions. *Lat. Am. Appl. Res*, *51*(4), (2021), pp. 229-239. https://doi.org/10.52292/j.laar.2021.523.
[22] Seid, E., *et al.*,. Multiple slip, Soret and Dufour effects in fluid flow near a vertical stretching sheet in the presence of magnetic nanoparticles. *International Journal of Thermofluids*, *13*, (2022), pp. 100136, https://doi.org/10.1016/j.ijft.2022.100136
[23] Nayak, M. K., *et al.*,.Entropy analysis of a 3D nonlinear radiative hybrid nanofluid flow between two parallel stretching permeable sheets with slip velocities. *International Journal of Ambient Energy*, *43*(1), (2022), pp. 8710-8721. https://doi.org/10.1080/01430750.2022.2101523
[24] Samanta Ray, S. S., *et al.*,. Darcy–Forchheimer up/downflow of entropy optimized radiative nanofluids with second-order slip, nonuniform source/sink, and shape effects. *Heat Transfer*, *51*(2), (2022), pp. 2318-2342. https://doi.org/10.1002/htj.22403
[25] Asmat, F., *et al.*, (2023). Thermal analysis in an electrically conducting fluid with multiple slips and radiation along a plate: a case study of Stokes' second problem. *Case Studies in Thermal Engineering*, *44*, (2023), pp. 102831. https://doi.org/10.1016/j.csite.2023.102831
[26] Shamshuddin, M. D., *et al.*,. Radiative and exponentially space-based thermal generation effects on an inclined hydromagnetic aqueous nanofluid flow past thermal slippage saturated porous media. *International Journal of Modern Physics B*, *37*(21), (2023), pp. 2350202. https://doi.org/10.1142/S0217979223502028
[27] Zhu, Y., and Granick, S.. No-slip boundary condition switches to partial slip when fluid contains surfactant. *Langmuir*, *18*(26), (2002), pp. 10058-10063. https://doi.org/10.1021/la026016f
[28] Wu, L.. A slip model for rarefied gas flows at arbitrary Knudsen number. *Applied Physics Letters*, *93*(25), (2008), pp. 1-12. http://digitalcommons.unl.edu/mechengfacpub/127
[29] Liao, S.. *Homotopy analysis method in nonlinear differential equations* (Vol. 153). (2012) Beijing: Higher education press.
[30] Verma, T. N., *et al.*,. Experimental and empirical investigation of a CI engine fuelled with blends of diesel and roselle biodiesel. *Scientific Reports*, *11*(1), (2021), pp. 18865. https://doi.org/10.1038/s41598-021-98382-1
[31] Agarwal, K. M., *et al.*,. Mechanical behaviour of Aluminium Alloy AA6063 processed through ECAP with optimum die design parameters. *Advances in Materials and Processing technologies*, *8*(2), (2022), 1901-1915. https://doi.org/10.1080/2374068X.2021.1878705
[32] Bandhu, D., *et al.*,. Experimental investigation and optimization of RMDTM welding parameters for ASTM A387 grade 11 steel. *Materials and Manufacturing Processes*, *36*(13), (2021), pp. 1524-1534. https://doi.org/10.1080/10426914.2020.1854472.

[33] Srikakulapu, R. *et al.,* Modelling farm-based electric vehicles on charging systems for power distribution networks with dynamic grid interactions. *Ain Shams Engineering Journal*, *14*(8), (2023), pp. 102046. https://doi.org/10.1016/j.asej.2022.102046.
[34] Nadeem, S., and Lee, C. Boundary layer flow of nanofluid over an exponentially stretching surface. *Nanoscale research letters*, *7*, (2012)., pp. 1-6. https://doi.org/10.1186/1556-276X-7-94
[35] Ishak, N., *et al.*, (2019,). Heat and mass transfer flow of a viscoelastic nanofluid over a stretching/shrinking sheet with slip condition. In *AIP conference proceedings* (Vol. 2059, No. 1). AIP Publishing.

Submitted: 24.4.2025.
Accepted: 11.6.2025.
Revised: 24.6.2025.